Mid-to-long wavelength IR emitters and detectors

Mike Cooke reports on attempts to improve quantum cascade emission and van der Waals semiconductor detection of MWIR and LWIR wavelengths.

The creation and detection of longer-wavelength infrared is challenging due to thermal effects. The mid-wavelength infrared (MWIR, 3–8μm) region corresponds to black-body temperatures of the order 362–966K, i.e. from 89°C up to 693°C. This range is useful for detecting jet engine exhausts in missile guidance systems, for example, since there is an atmospheric window for this range of wavelengths with relatively low absorption.

The long-wavelength infrared range (LWIR, 8–15μm) can be used for thermal imaging with black-body temperatures of the order 193–362K (–80°C–+89°C) covering the normal range that humans expect to encounter and more.

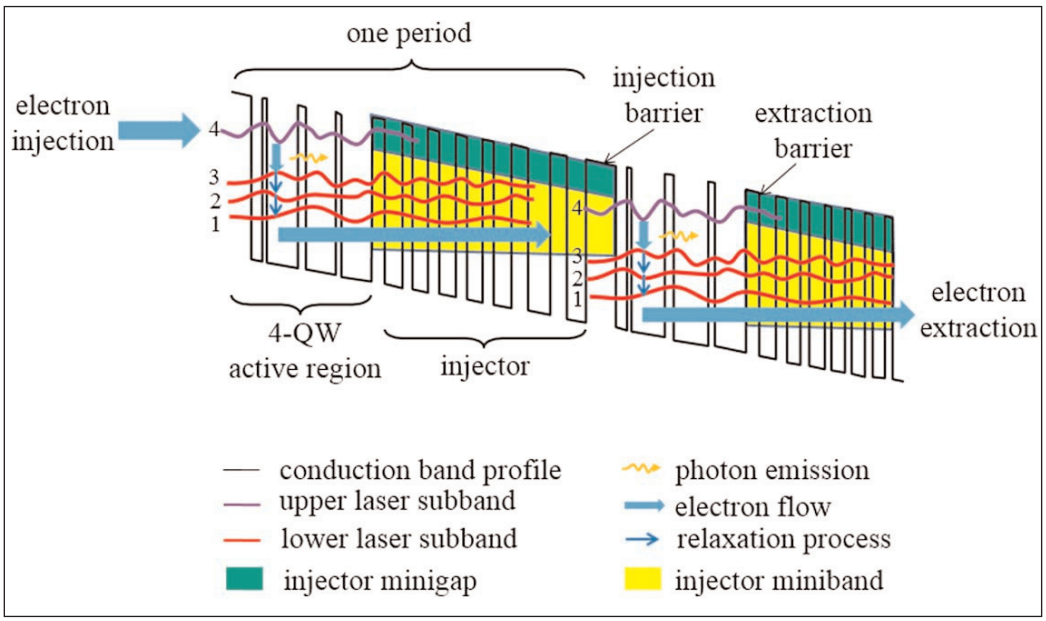

Figure 1. Band structure of four-QW coupling and two-phonon-resonance-based QC energy level.

Of course, if the equipment is expected to operate at 'room temperature', there will be problems separating useful signals from background noise. Usually this is accomplished by cooling the equipment relative to the surroundings. Alternatively one can reduce the relative importance of ambient noise by using additional appropriate illumination.

Here we look at some recent research in improving semiconductor-based mid-to-long wavelength infrared illumination and detection.

Quantum cascade superluminescent arrays

Researchers based in China have developed ~5μm-wavelength mid-infrared quantum cascade superluminescent emitters (QCSLE), in single and array formats [Jialin Sun et al, Optics Letters, vol43, p5150, 2018]. The team from Suzhou Institute of Nano-Tech and Nano-Bionics (SINANO), Institute of Semiconductors, and University of Science and Technology of China, sees potential for biomedical imaging, security inspection and gas detection from using QCSLEs as broadband light sources.

A particular application could be optical coherence tomography (OCT), which is widely used for human tissue imaging. In the near-infrared (NIR) such techniques have achieved high resolution in a non-invasive, non-contact manner. The team comments: "It is noteworthy that most biological tissues absorb much more photons within the mid-infrared (MIR) spectral range compared to the NIR range, indicating that a MIR-OCT could contain strong overtone and combination vibrational absorption bands of the spectral response to molecular species."

The paper reports "for the first time, to the best of our knowledge" a compact light-emitter array with a very high room-temperature continuous wave (RT-CW) light output power of 2.4mW. Such RT-CW operation is seen as a crucial requirement for MIR-OCT.

Superluminescent devices use amplified spontaneous emission to give high-power, low-coherence light. SLEs use a single-pass structure so spontaneous photons are amplified, but lasing does not occur. To ensure single-pass behavior, it is necessary that the waveguide structure transmits light out, rather than the photons being trapped in multiple reflections, as in lasers.

The active layers of the QC structure were grown by solid-source molecular beam epitaxy (SS-MBE) on indium phosphide. The active region of the cascade

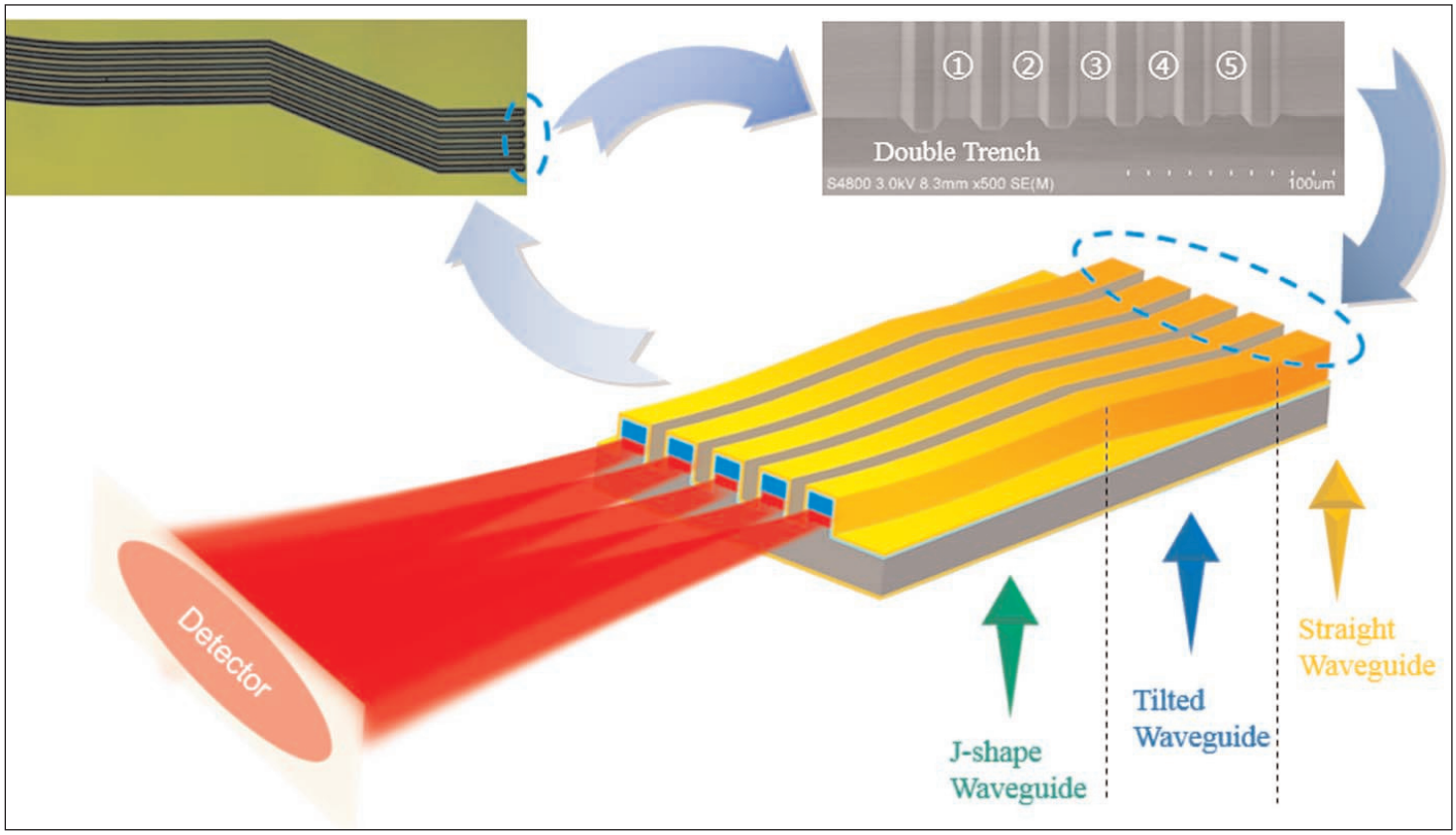

Figure 2. Bottom: schematic diagram of array device. Top-left: microscope image of 5-array. Top-right: corresponding scanning electron microscope image of rear end.

section (Figure 1) was four coupled strain-compensated quantum wells (QWs) of indium gallium arsenide in indium aluminium arsenide ($In_{0.678}Ga_{0.322}As/In_{0.365}Al_{0.635}As$). The structure used a two-phonon resonance structure to improve depopulation of the lower state, enabling increased amplification from stimulated emission. At the same time, the four wells enhanced spontaneous emission. The device material consisted of 30 repetitions of the cascade section design separated by low-doped n-InGaAs. The target emission wavelength was ~5μm.

The material was fabricated into double-trench narrow-ridge 'W'-shaped waveguide structures 7μm deep. The ridge width was 10μm and the trench widths were 20μm. Plasma-enhanced chemical vapor deposition (PECVD) silicon dioxide, 200nm thick, was used as insulation. Contact windows, 3μm wide, were etched in a reactive-ion process. The top contact metals were titanium/gold. The bottom contact consisted of germanium/gold/nickel/gold. The devices were mounted epitaxial-side down on copper heat-sinks.

The waveguide was shaped with a 1mm-long tilted section connected to 0.5mm-long straight and 2mm-long 'J' sections (Figure 2, SLE 1). The researchers comment: "This design can create two mutations of refractive index in the waveguide to achieve a rather low reflectivity with a fairly small geometry, and hence provide an opportunity to fabricate array devices."

Two further devices (SLE 2 and SLE 3) were produced giving a shorter 'J' section of 1.5mm. This reduced the angle between the tangent to the end of the 'J'-section and the output facet normal from 9° to 4°. One of these latter devices also included a high-reflection coating on the rear facet (SLE 3).

The maximum output powers for three different structures were 1.6mW (at 1.75A, SLE 1), 2.2mW (at 1.85A, SLE 2) and 3mW (at 1.9A, SLE 3). The slope efficiency of SLE 3 was 0.0028W/A, about twice that of SLE 1.

Compact SLE arrays with up to 7 devices were based on the SLE 3 structure. The arrays were characterized in 'quasi-continuous wave' mode — 5μs pulses with 20kHz repetition (10% duty cycle) — at room temperature. The best performances were delivered by 3-SLE and 5-SLE arrays: 8.5mW output at 5.5A and 12mW output at 7A, respectively. The 7-array suffered from "excess thermal generation and low current density". The turn-on voltage of the 7-array was ~12V, compared with ~9V for a single SLE 3 device.

Continuous-wave operation of the 5-array gave an output power of 2.4mW at 3A with 199/cm full-width at half maximum (FWHM) — see Figure 3. The researchers comment: "The high output power can increase the penetrating depth of light, the broad spectral width can enhance the axial resolution of the images, and the high-quality output beam can be effectively coupled into fiber, so the QC array device has been demonstrated as an ideal broadband light source for realizing the MIR-OCT system."

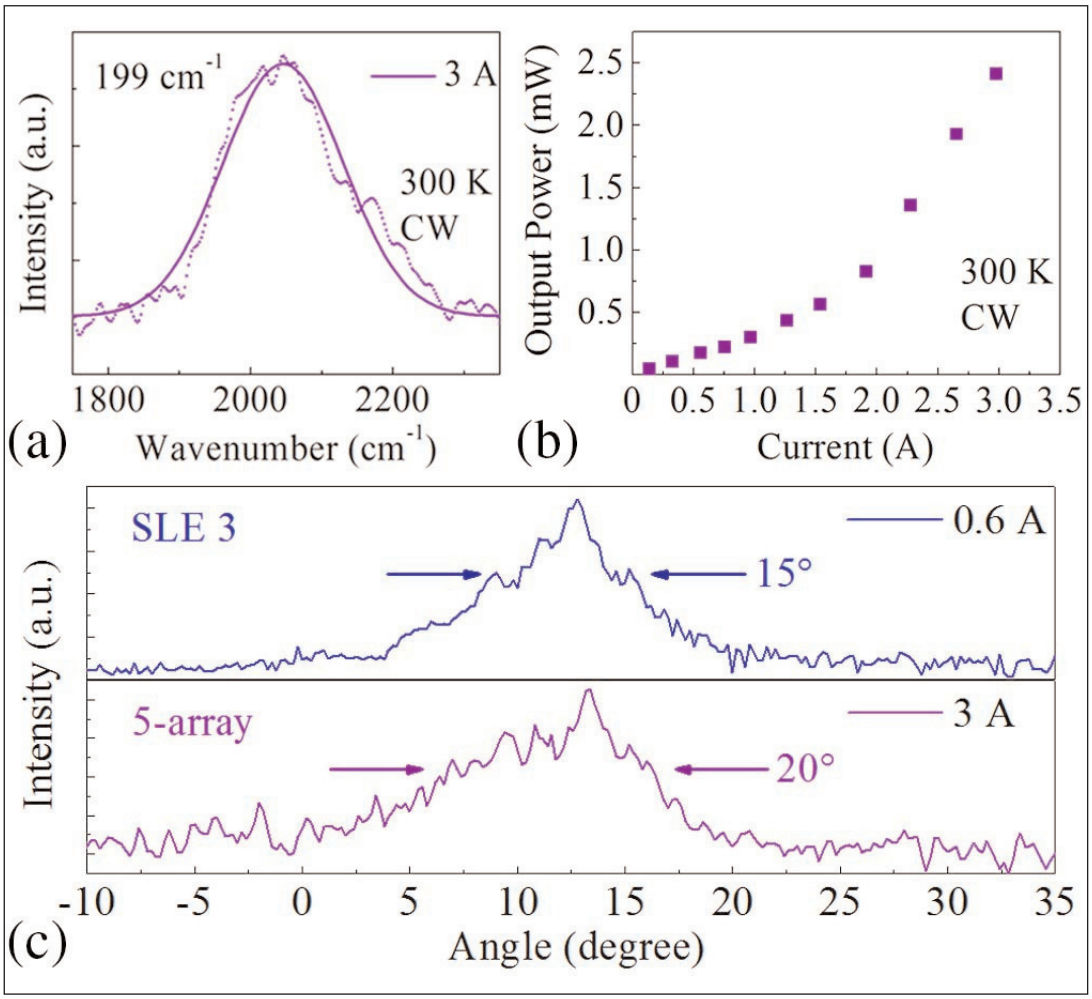

Figure 3. (a) Emission spectrum and (b) light–current curve measured from 5-array under CW mode at 300K. Lines corresponding to Gaussian fitting to spectra. (c) Comparisons between far-field profiles of SLE 3-array and 5-array.

Reorienting quantum cascade lasers

Humboldt University Berlin and Paul-Drude-Institut für Festkörperelektronik in Germany have used (411)A-oriented indium phosphide (InP) to improve the power efficiency, threshold current and slope efficiency of quantum cascade lasers (QCLs) [M. P. Semtsiv et al, Appl. Phys. Lett., vol113, p121110, 2018]. Targeted at 9μm-wavelength emission, the material used combinations of indium gallium arsenide (InGaAs) and indium aluminium arsenide (InAlAs) layers.

The researchers attribute the improvements to reduced interface roughness (IFR) scattering enabled by growth on (411)A material, compared with conventional on-axis (100) substrates. "Reduced IFR scattering results in better inversion, longer upper laser state lifetime, smaller non-radiative recombination, and less leakage current during injection," the team reports.

The improvements are thought to result from the change in average lateral extent of the roughness, rather than the height/amplitude. The lateral extent for the conventional (100) orientation is around 6nm, which gives expect peak expected IFR scattering in devices aimed at 9–20μm-wavelength emission.

The researchers report that, although off-cut substrates like (411)A InP are commonly used to achieve almost atomically flat epitaxial growth fronts, they had not been previously applied in QCL work. The team explains: "The off-cut substrates introduce monolayer-high steps into the growth front, but these steps are more regular than the random monolayer-high islands on the exact (100) surface, and are characterized by a different lateral size Λ. Growth proceeds in the step-flow mode, reducing fluctuations with random lateral extent."

The (411)A orientation is tilted 19.5° relative to the convention (100) surface plane in the [011] direction. The flat surface morphology during epitaxy has typically 1.8nm-long terraces in the [$\bar{1}$22] direction, much shorter than the 6nm 'lateral extent' seen for the (100) orientation. Previous work characterizing such material confirmed improved qualities such as higher electron mobility and a narrower photoluminescence peak.

The epitaxial wafers were produced on InP substrates with conventional (100) and with (411)A surface orientations. The QCL epitaxial structure, based on a design by Hamamatsu Photonics K.K. researchers, was an InGaAs/InAlAs heterosystem lattice-matched to InP, giving a dual-upper-state to multiple-lower-state active regions. The growth temperature was 500°C.

The material was fabricated into lasers with ~30μm-wide ridges. For the (411)A, the ridge was oriented along the [1$\bar{1}$0] crystal direction, allowing cleavage along the perpendicular direction to give mirror facets. The ridge sidewalls were insulated with silicon dioxide. The top and bottom electrodes were annealed chromium/gold and gold-germanium/chromium/gold, respectively. The devices were soldered onto copper-tungsten submounts.

Although the devices operated at room temperature and above, the reported measurements were restricted to the stable 60–280K range of the team's cryostat equipment. The team believes, however, that

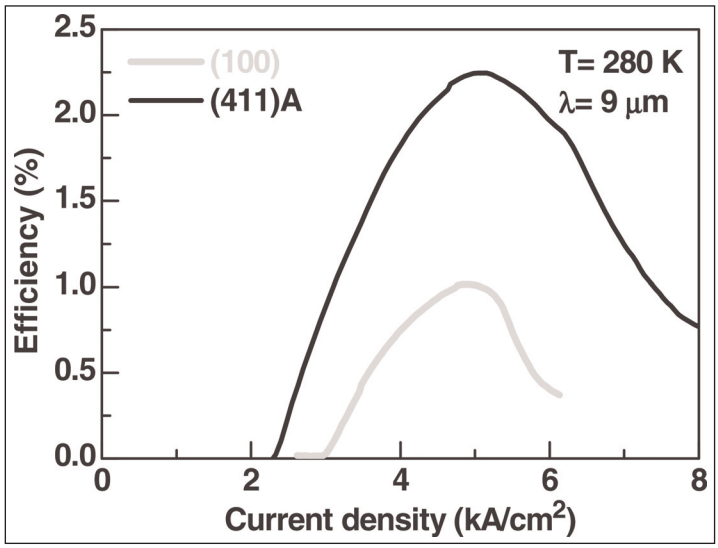

Figure 4. Power (wall plug) efficiency as a function of current density with the same QCL structures grown on (411)A- and (100)-oriented InP. Both lasers were 4mm long. Lasers grown on (411)A and (100) substrates had 24.4μm- and 32.7μm-wide ridges, respectively.

the efficiency improvements enabled by growth on (411)A InP could result in higher maximum operation temperatures.

The (411)A device demonstrated more than twice the maximum 'wall-plug' power efficiency at 280K under 150ns pulsed operation with 10kHz repetition, compared with the reference (100) QCL (Figure 4). The improvement is credited to reduced interface roughness scattering. The threshold currents of the (411)A devices were also lower (Figure 5). However, the lower characteristic temperature for the threshold (T_0) for the (411)A QCL does mean that the threshold does approach that of the conventional (100) laser at higher temperatures. The researchers attribute this to "an increasing influence of phonon scattering".

Above 150K the slope efficiency of the (411)A device was about 50% higher than that of the (100) structure. The saturation of the (411)A QCL's slope efficiency below 150K was probably due to freeze-out of carriers as a result of the low doping used in the design, the researchers suggest. A (411)A QCL with a wider 33.2μm ridge had similar temperature characteristics: 217K for T_0, and 234K for the slope efficiency (T_1).

The researchers suggest that these efficiency improvements could result in higher maximum operation temperatures also for longer-wavelength 'terahertz' long-wavelength and far-infrared devices.

Black phosphorus photodiode

Researchers based in the USA, Taiwan and Australia have improved the performance of mid-wavelength infrared (MWIR, 3–8μm) photodiodes using black

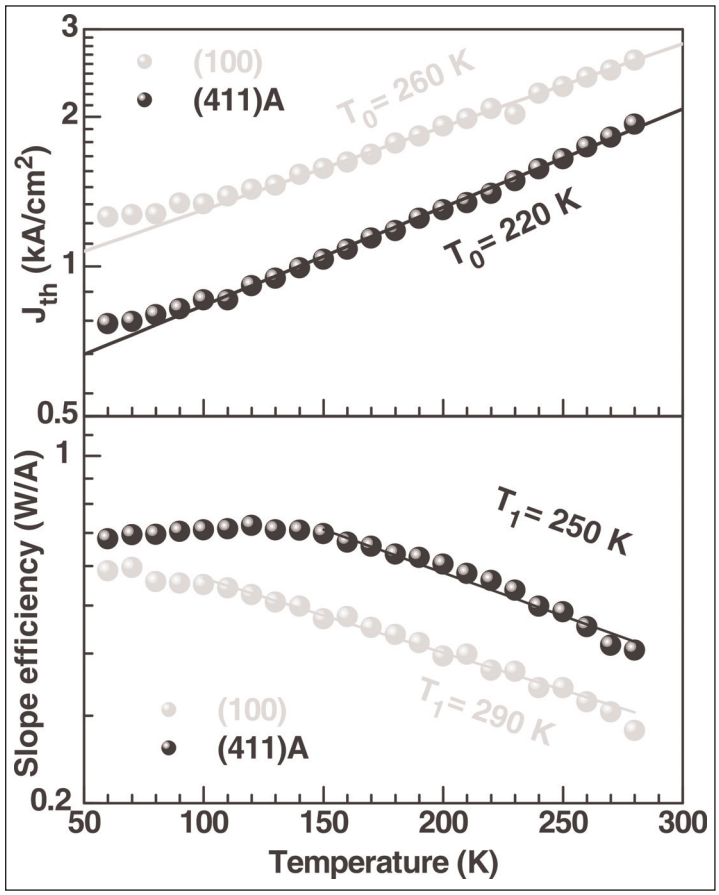

Figure 5. Top: threshold current densities as functions of temperature for QCLs on (411)A and (100) InP. Bottom: slope efficiency functions of temperature. In both panels, bullets are experimental data and lines are simple exponential fits.

phosphorus (bP) as absorbing material and a molybdenum disulfide (MoS_2) electrode [James Bullock et al, Nature Photonics, published online 27 August 2018].

The team from University of California Berkeley and Lawrence Berkeley National Laboratory (LBNL) in the USA, Taiwan's National Tsing Hua University and Australia's University of Melbourne claim that their devices can be competitive with conventional MWIR detectors. Further, the team used the anisotropic optical response of black phosphorus to "demonstrate the first bias-selectable polarization-resolved photodetector that operates without the need for external optics," with potential for astronomy, polarization-division multiplexing and remote sensing.

'Van der Waals' materials such as black phosphorus and MoS_2 have many interesting properties due to their two-dimensional (2D) nature of strong in-plane bonds but weaker between-plane bonds. The Van der Waals forces between planes avoid problems with 'dangling bonds' at the surface that can cause difficulties with devices based on conventional 3D bulk semiconductor materials. The 2D materials can be used to create thin absorbing layers with reduced noise from thermal electron-hole generation-recombination. Bulk

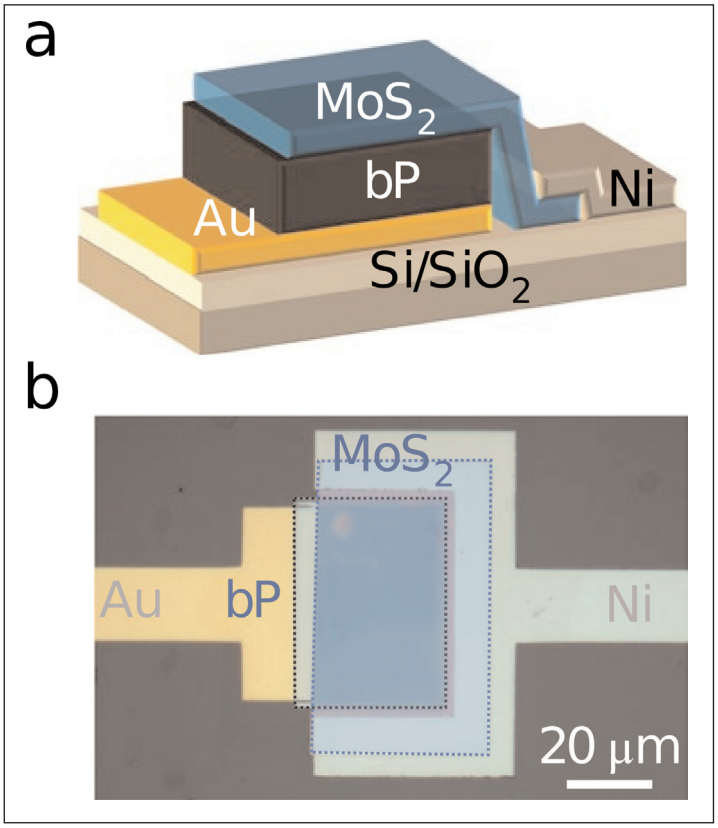

Figure 6. bP/MoS_2 heterojunction photodiode concept. a, Schematic of device configuration, showing the heterojunction and contact configuration. b, Optical micrograph of a completed device; regions containing black phosphorus and MoS_2 are outlined for clarity.

semiconductor layers need to be thicker to reduce the effect of surface recombination at their problematic dangling bonds.

The bandgap of black phosphorus ranges from 1.5eV for monolayers shifting down to 0.3eV as the thickness increases, putting longer and longer wavelengths into the detectable range (~830nm out to ~4.1μm). At the same time, MoS_2 is also a 2D Van der Waals material from the transition-metal dichalcogenide family.

The researchers are looking to MWIR applications in the medical, scientific, communication, automation and surveillance fields. They hope that the use of black phosphorus as absorber could overcome problems with other technologies such as expensive processing and the need for costly active cooling to reduce thermal noise.

The devices consisted of a back pad/reflector of gold, black phosphorus, and a top window/contact of 10–20nm n-type MoS_2 (Figure 6). The band offset between the black phosphorus and n-MoS_2 enables electron flow into the contact material, but blocks holes. The monolayer thicknesses of black phosphorus and MoS_2 were 5.5Å and 6Å, respectively. Electron microscope analysis suggested some amorphous material at the bP/MoS_2 interface, which was attributed

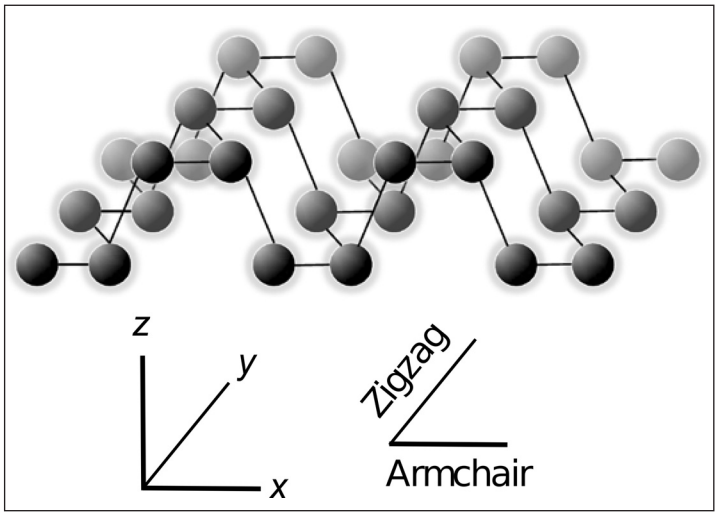

Figure 7. Schematic diagram of black phosphorus crystal structure.

to oxidation of the phosphorus due to air exposure during fabrication. The design of the device was optimized using simulations.

The optimum structure was expected to be 150nm black phosphorus and 15nm MoS_2, giving a predicted ~80% absorption of polarized light at 3μm wavelength. The optimum polarization was along the 'x' or 'armchair' direction of the black phosphorus atomic structure (Figure 7). The moderately thin black phosphorus layer should reduce noise while still permitting high absorption in the narrow MWIR target spectral range.

A fabricated device demonstrated a peak external quantum efficiency (ε_e) between 30% and 35% for radiation wavelengths between 2.5μm and 3.5μm (Figure 8). The researchers comment: "These are the highest ε_e values reported for black phosphorus in this range at room temperature and correspond to current-responsivity values of ~0.9AW^{-1}." Previous work has only managed ee values less than 5% in the near-infrared and short-wavelength infrared regions.

The device design targeted a quarter-wavelength interference peak at just below 3μm. The internal quantum efficiency (ε_i) was estimated to be 40–50%. Moving the polarization of the incident radiation from the x to y ('zig-zag') directions reduced ε_e from more than 30% down to less than 1%. Reducing the operating temperature to 78K increased ε_e to 63% for 3μm infrared.

The detectivity (D*) peaked at 3.8μm with a value of $1.1x10^{10}cmHz^{1/2}/W$, according to an estimate based on the zero-bias resistance area product. Unlike many more established technologies, the device was not biased to improve performance. A measurement based on noise equivalent power measurements under flood illumination from a black-body source (from 100°C up to 400°C) gave a D* value of $7x10^{9}cmHz^{1/2}/W$. The researchers consider the agreement between the two methods to be 'good'.

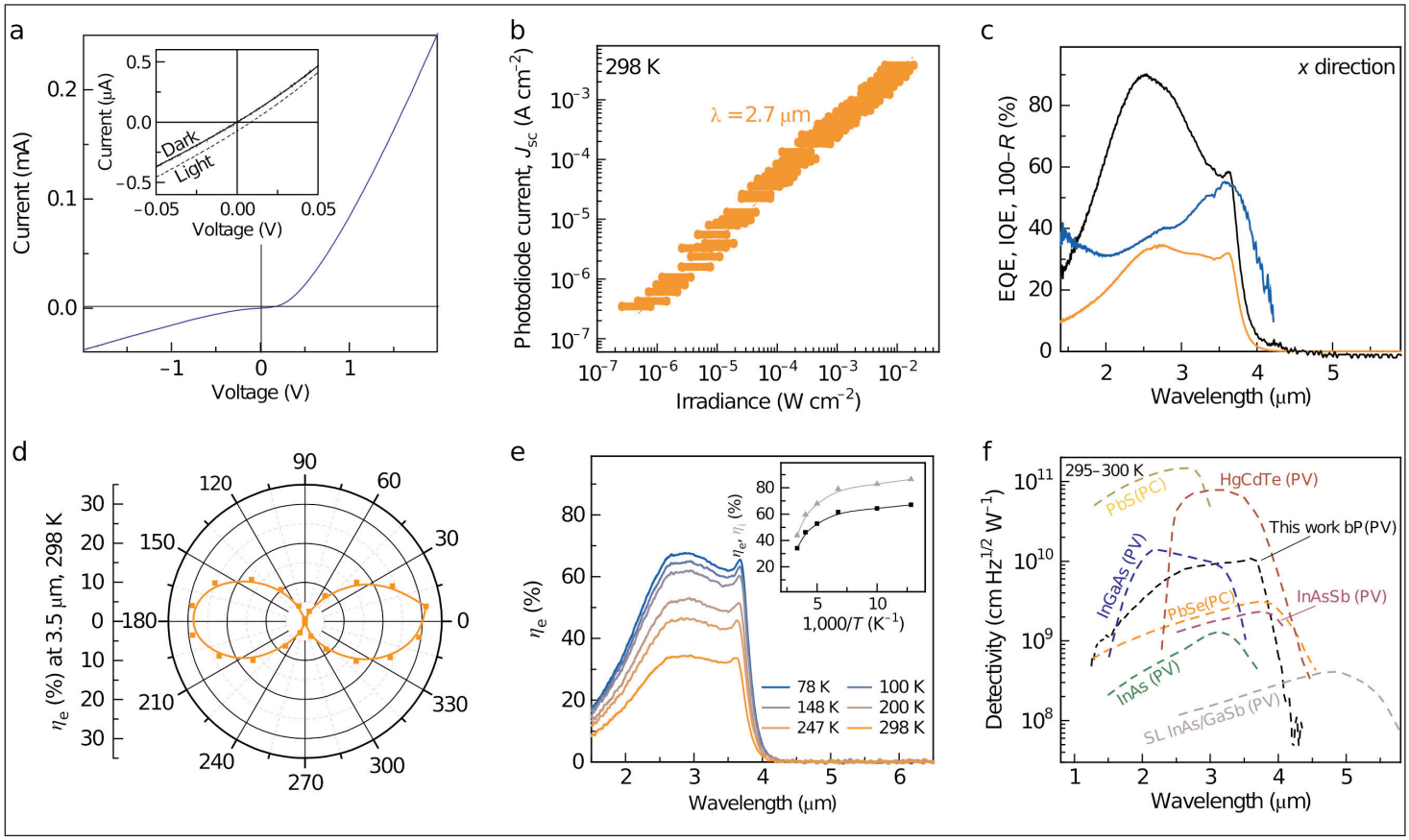

Figure 8. Photoresponse and detectivity characterization performed at zero bias. a, Current–voltage curve with inset measurements in dark and under illumination by 1000K black-body source. b, Measured photocurrent as function of incident illumination intensity with2.7μm laser diode source. Error bars represent uncertainty in spot size. c, Spectrally dependent ε_e, ε_i and 100%-reflectivity (R). d, Variation of ε_e with polarization angle at 3.5μm wavelength. e, Spectral ε_e as a function of temperature with inset ε_e and ε_i variation at 3μm. f, Specific detectivity versus wavelength at room temperature as well as various commercially available and reported MWIR photovoltaic (PV) and photoconductive (PC) detectors.

The rise-time and fall-time responses to 2.7μm infrared were 3.7μs and 4.0μs, respectively, "among the fastest reported for bP-based photoconductors and photodiodes," according to the team. However, commercial devices have faster response, and the researchers hope that improvements could come from reducing the bP bulk trap concentration and eliminating defective interfacial layers with oxidant-free fabrication.

A more complex device was developed for polarization resolution. Two layers of black phosphorus with perpendicular crystal alignments were separated by a MoS_2 electrode (Figure 9). The bottom black phosphorus had a gold contact, while the top black phosphorus layer used a stack of molybdenum oxide and palladium (MoO_x/Pd) to collect holes. The arrangement allowed discrimination between radiation polarized in the two different directions. ■

Author:
Mike Cooke is a freelance technology journalist who has worked in the semiconductor and advanced technology sectors since 1997.

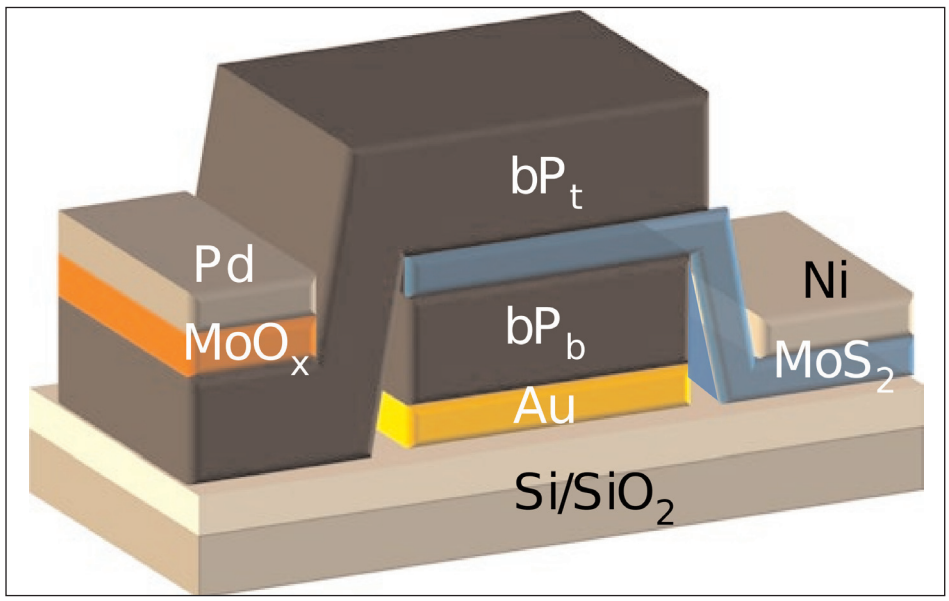

Figure 9. Polarization-resolved bP/MoS_2 heterojunction photodiode.